Electronic Supporting Information

Mechanochemical Synthesis of Pure Phase Mixed-cation/Anion $(FAPbI_3)_x(MAPbBr_3)_{1-x}$ Hybrid Perovskite Materials: Compositional Engineering and Photovoltaic Performance

Sheng Tang,‡[a] Xinyu Xiao,‡[a] Jing Hu,[a] Bo Gao,[a] Hunglin Chen,[a] Zhuang Zuo,[a] Qi Qi,[a] Zongyang Peng,[a] Jianchun Wen[a] and Dechun Zou*[ab]

*Corresponding authors

[a]Beijing National Laboratory for Molecular Sciences, Key Laboratory of Polymer Chemistry and Physics of Ministry of Education, Center for Soft Matter Science and Engineering, College of Chemistry and Molecular Engineering, Peking University, Beijing 100871, China, E-mail: dczou@pku.edu.cn.

[b]Beijing Engineering Research Center for Active Matrix Display, Peking University, Beijing 100871, China.

Table S1 Relative atomic ratio of Pb, I and Br for $(\alpha\text{-}FAPbI_3)_x(MAPbBr_3)_{1-x}$ powders and films found from EDX measurements.

x	Atomic Ratio					
	powder			film		
	Pb	I	Br	Pb	I	Br
0	1.0	0	3.0	1.0	0	2.9
0.1	1.0	0.3	2.8	1.0	0.3	2.6
0.2	1.0	0.5	2.5	1.0	0.6	2.4
0.3	1.0	0.9	2.1	1.0	0.9	2.2
0.4	1.0	1.1	1.9	1.0	1.1	1.9
0.5	1.0	1.3	1.6	1.0	1.5	1.6
0.6	1.0	1.6	1.2	1.0	1.9	1.3
0.7	1.0	2.1	0.9	1.0	2.4	0.9
0.8	1.0	2.5	0.6	1.0	2.7	0.6
0.9	1.0	2.6	0.3	1.0	3.3	0.3
1.0	1.0	3.0	0	1.0	2.9	0

Table S2 Optical properties of $(\alpha\text{-}FAPbI_3)_x(MAPbBr_3)_{1-x}$ powders and films.

$(\alpha\text{-}FAPbI_3)_x(MAPbBr_3)_{1-x}$	powder		film	
	λ_{onset}/nm	E_g/eV	λ_{onset}/nm	E_g/eV
0	563	2.21	537	2.31
0.1	595	2.08	563	2.20
0.2	634	1.96	580	2.14
0.3	664	1.87	610	2.03
0.4	696	1.78	638	1.94
0.5	717	1.73	670	1.85
0.6	749	1.66	697	1.78
0.7	775	1.60	725	1.71
0.8	806	1.54	758	1.64
0.9	828	1.50	793	1.56
1.0	861	1.44	815	1.52

Table S3 Optical properties of $(\delta\text{-}FAPbI_3)_x(MAPbBr_3)_{1-x}$ powders.

$(\delta\text{-}FAPbI_3)_x(MAPbBr_3)_{1-x}$	λ_{onset}/nm	E_g/eV
0	563	2.21
0.1	596	2.08
0.2	623	1.99
0.3	660	1.88
0.4	697	1.78
0.5	713	1.74
0.6	731	1.69
0.7	770	1.61
0.8	797	1.56
0.9	827	1.50
1.0	560	2.21

Table S4 Thermal decomposition temperature of $(\alpha\text{-}FAPbI_3)_x(MAPbBr_3)_{1-x}$ and $(\delta\text{-}FAPbI_3)_x(MAPbBr_3)_{1-x}$ powders tested by TGA.

x	T_d/℃	
	$(\alpha\text{-}FAPbI_3)_x(MAPbBr_3)_{1-x}$	$(\delta\text{-}FAPbI_3)_x(MAPbBr_3)_{1-x}$
0	226	226
0.1	236	240
0.2	241	244
0.3	252	255
0.4	257	253
0.5	269	250
0.6	265	258
0.7	274	271
0.8	293	289
0.9	299	297
1.0	300	300

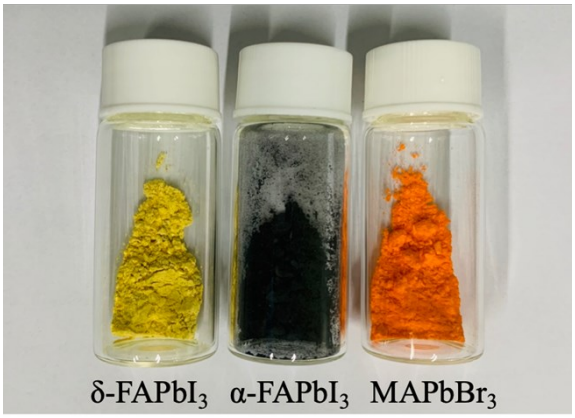

Fig. S1 Photographs of δ-$FAPbI_3$ (yellow), α-$FAPbI_3$ (black) and $MAPbBr_3$ (orange).

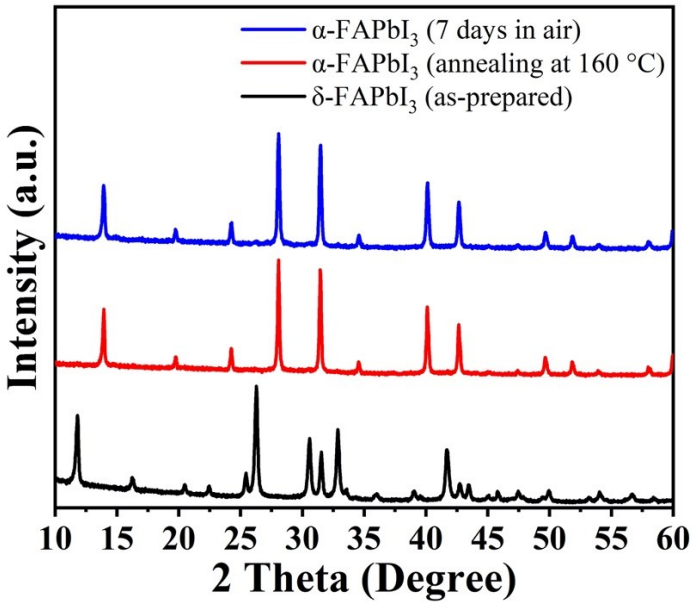

Fig. S2 XRD spectra of $FAPbI_3$ powders. The mechanical-prepared yellow δ-$FAPbI_3$ powder shows a non-perovskite phase and is converted to the black perovskite phase after being annealed at 160 °C for 60 min. The α-$FAPbI_3$ powder remains in the black perovskite phase after being stored in air for 7 days, which shows good thermal stability.

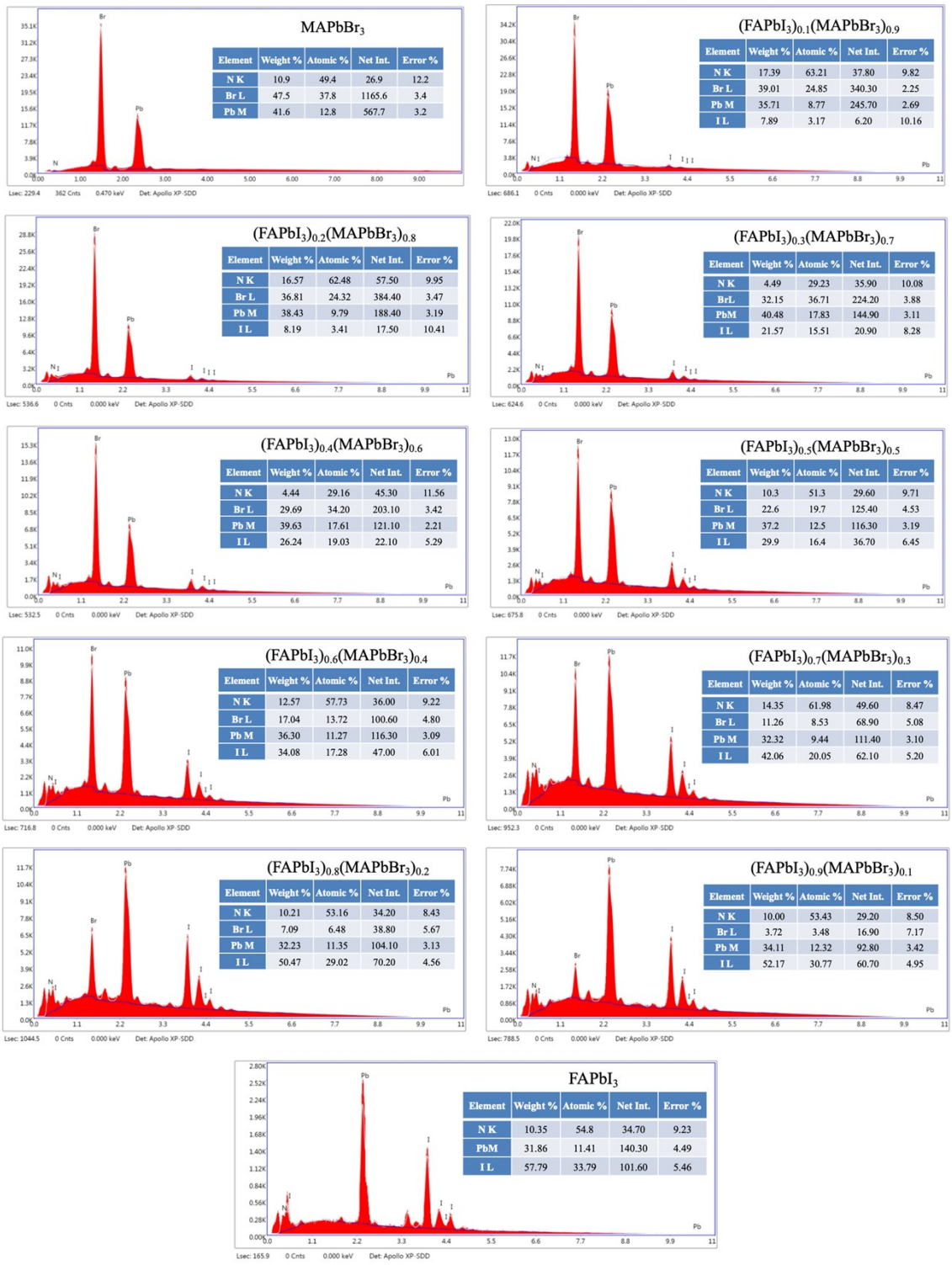

Fig. S3 EDX elemental spectra of $(\alpha\text{-}FAPbI_3)_x(MAPbBr_3)_{1-x}$ (x = 0, 0.1, …, 0.9, 1.0) powders prepared by MCS. Insert: atomic ratios of elements N, Br, I and Pb.

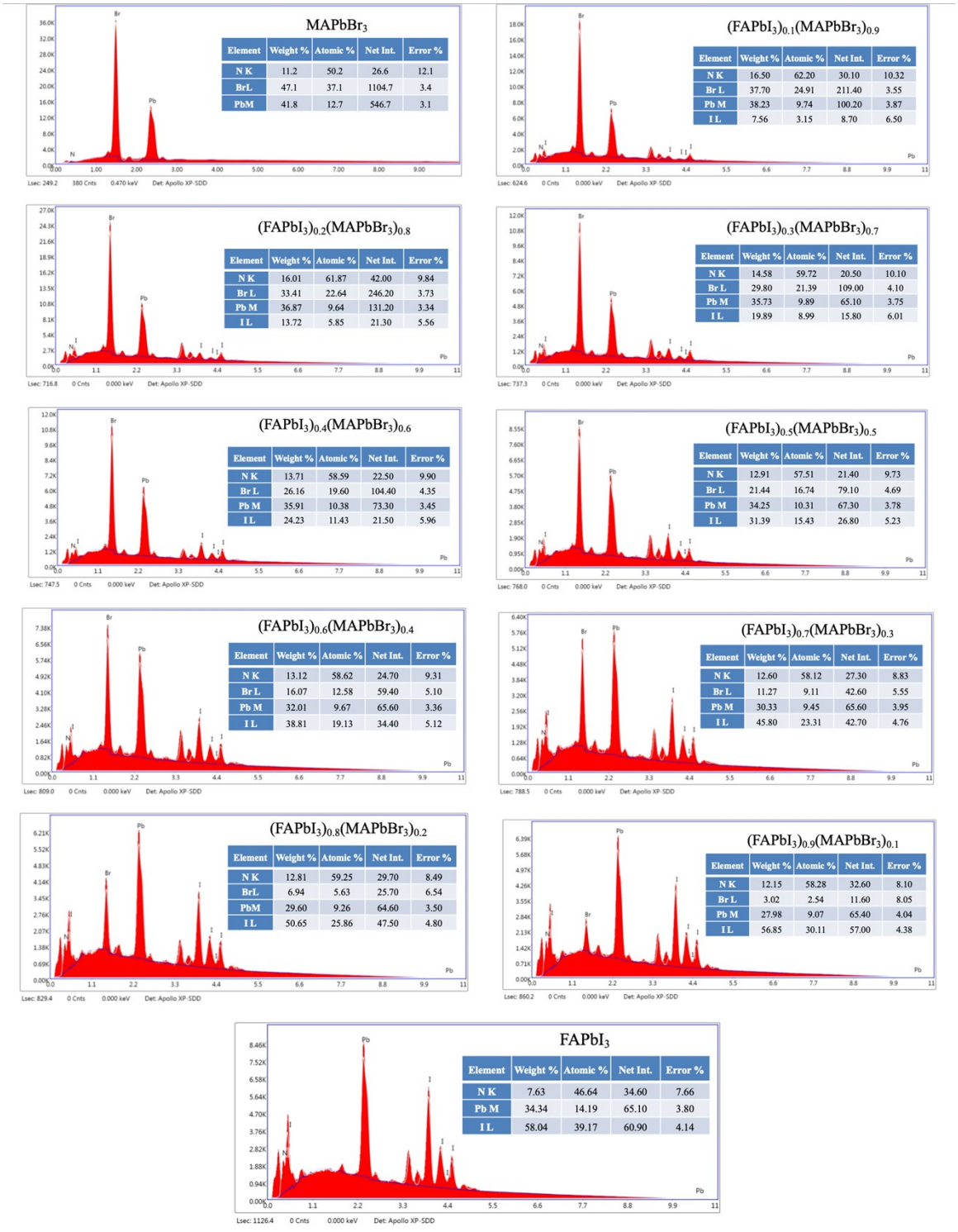

Fig. S4 EDX elemental spectra of (α-$FAPbI_3$)$_x$($MAPbBr_3$)$_{1-x}$ (x = 0, 0.1, …, 0.9, 1.0) films prepared by MCS. Insert: atomic ratios of elements N, Br, I and Pb.

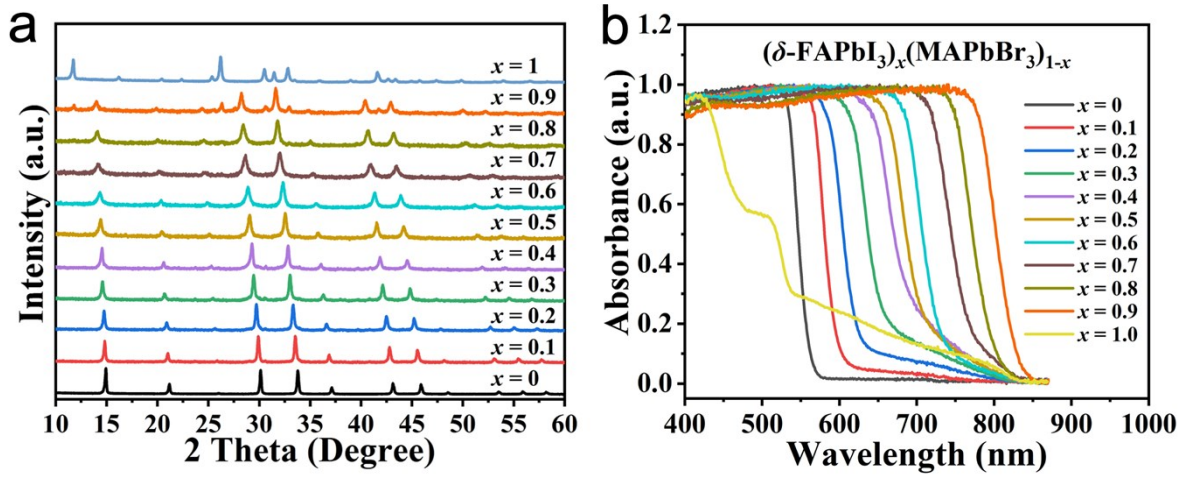

Fig. S5 (a) XRD patterns and (b) UV–vis absorption spectra of $(\delta\text{-FAPbI}_3)_x(\text{MAPbBr}_3)_{1-x}$ ($0 \le x \le 1$) perovskite powders prepared by MCS.

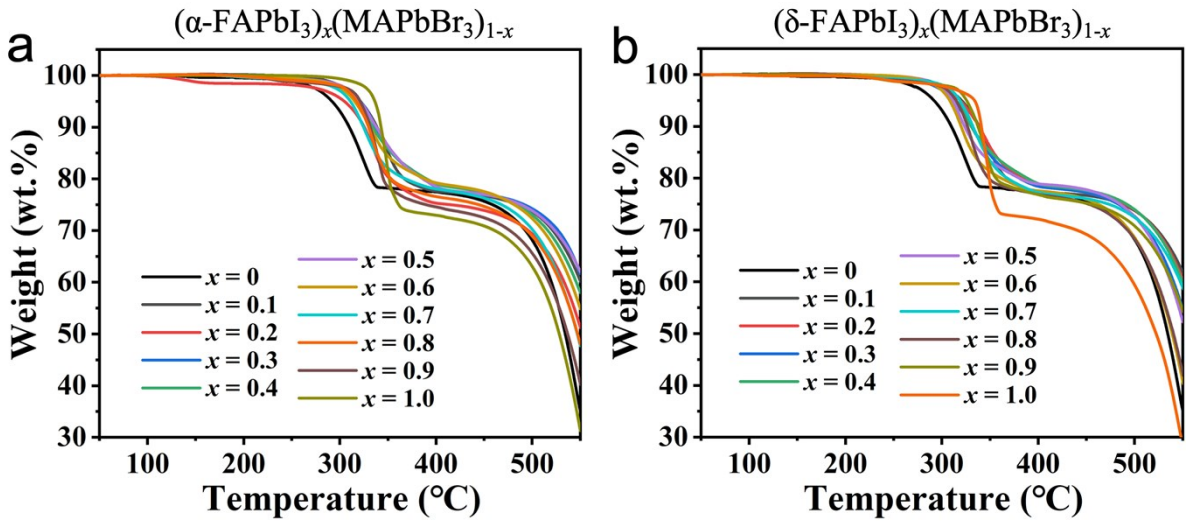

Fig. S6 Thermal stability of the perovskite powders prepared by MCS. TGA curves of (a) $(\alpha\text{-FAPbI}_3)_x(\text{MAPbBr}_3)_{1-x}$ and (b) $(\delta\text{-FAPbI}_3)_x(\text{MAPbBr}_3)_{1-x}$ (x = 0, 0.1, …, 0.9, 1.0).

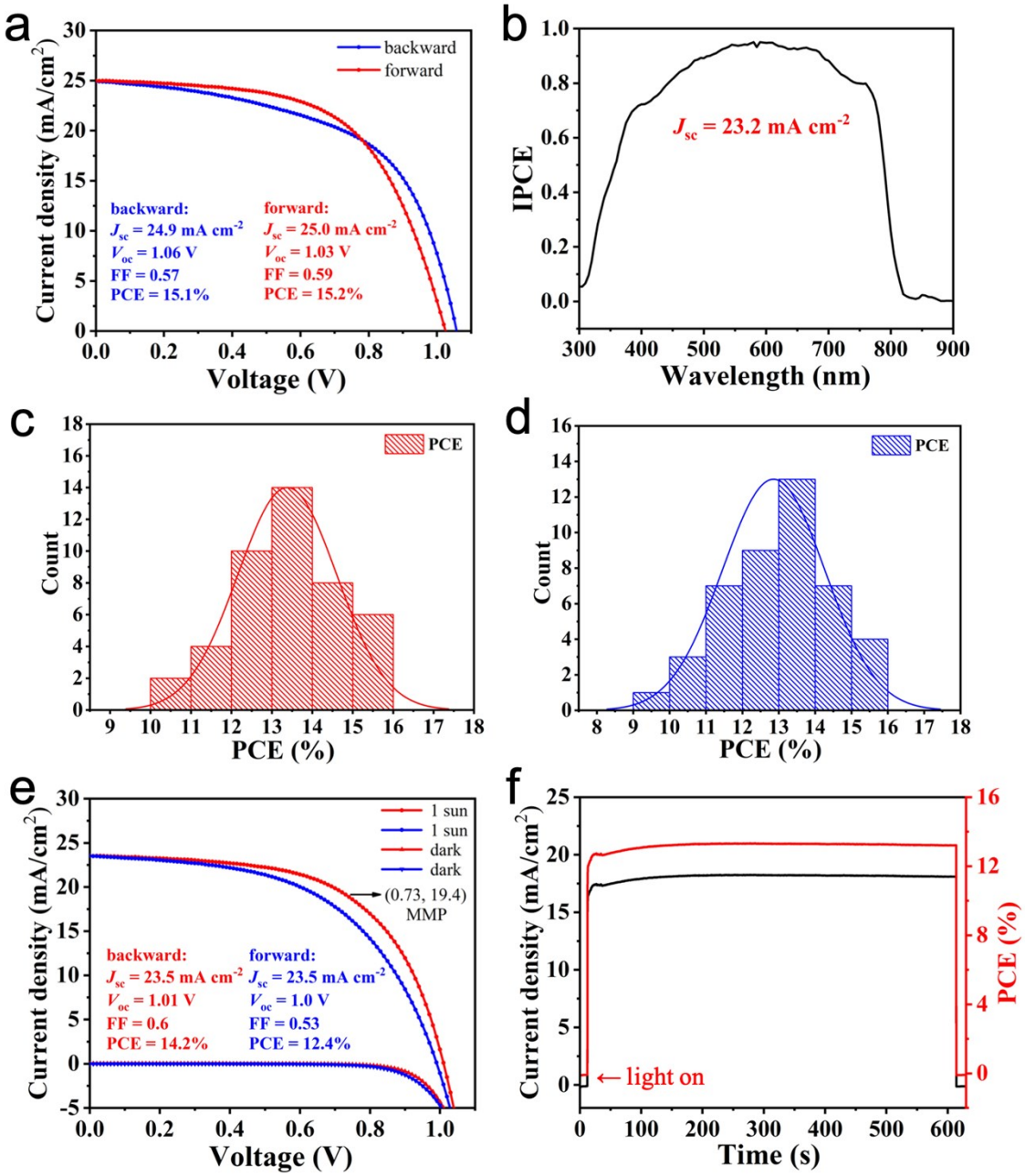

Fig. S7 (a) *J–V* curves of the best performance solar cell under forward and backward scans by using FAI, PbI_2, MABr and $PbBr_2$ in the corresponding ratio of $(\alpha\text{-}FAPbI_3)_{0.95}(MAPbBr_3)_{0.05}$ prepared by SS; (b) IPCE test result and integrated J_{sc} value; cell efficiency distributions; (c) backward scan; (d) forward scan; (e) *J–V* curves of the cell for steady-state output test; (f) steady-state current density and PCE continuous output of the tested cell at maximum power point (MMP) for 600 s.

Fig. S6a shows representative *J–V* curves of PSCs made from SS method, with a PCE of 15.2% (forward scan, V_{oc}, J_{sc} and FF being 1.03 V, 25.0 mA cm^{-2} and 0.59, respectively) and 15.1% (backward scan, V_{oc}, J_{sc} and FF being 1.06 V, 24.9 mA cm^{-2} and 0.57, respectively). The devices show strong hysteresis. The IPCE spectrum demonstrates a high photon-to-current

conversion efficiency from 400 nm to 800 nm. The integration of the IPCE over the AM 1.5 G spectrum yields a photocurrent density of 23.2 mA cm^{-2} (Fig. S6b), which is close to the short circuit photocurrent density of 24.9 mA cm^{-2} derived from the *J–V* curve. Under the optimal conditions, the power conversion efficiency distributions of the obtained devices are shown in Fig. S6c (backward scan) and Fig. S6d (forward scan). The PCE distributions are 10%−16% (backward scan) and 9%−16% (forward scan). The average PCEs are 13.4% (backward scan) and 12.9% (forward scan). The stabilised maximum power output measurements presented in Fig. S6e and Fig. S6f show good agreement between the measured PCE and the power output. When applying a constant voltage of 0.73 V corresponding to the maximum power point (MMP), the output current density is stable at 18.0 mA cm^{-2} under the continuous output test for 600 s, and the corresponding power conversion efficiency is 13.2%, thereby showing good continuous output stability.

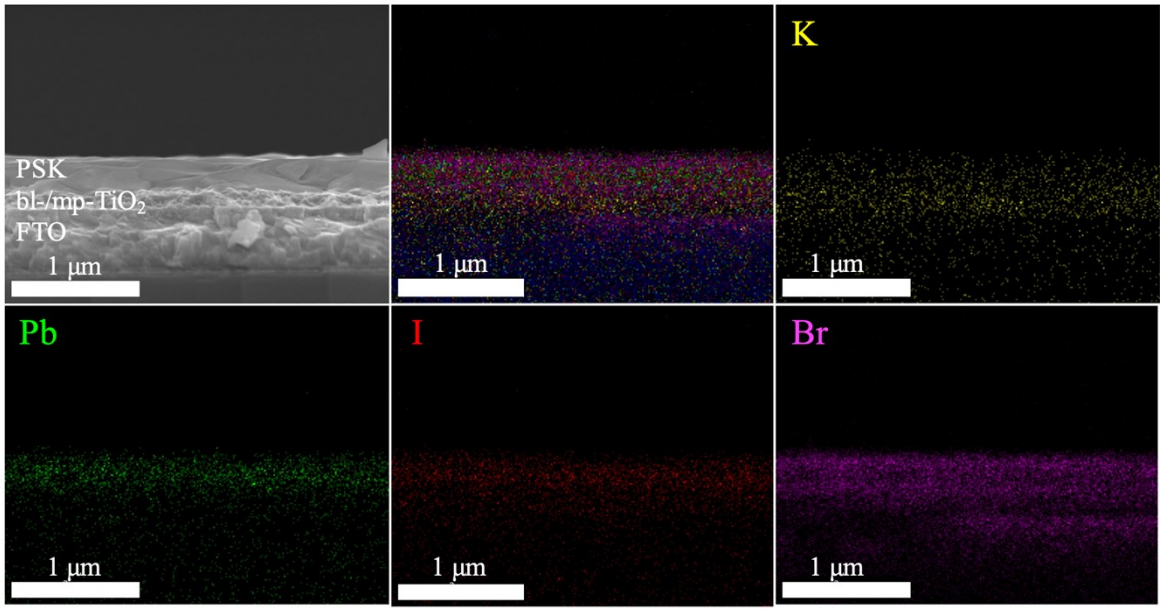

Fig. S8 SEM cross-sectional and EDX elemental mapping images demonstrate the homogeneous distribution of K, Pb, I and Br in the $(KPbI_3)_{0.05}(FAPbI_3)_{0.9}(MAPbBr_3)_{0.05}$ film (BM).

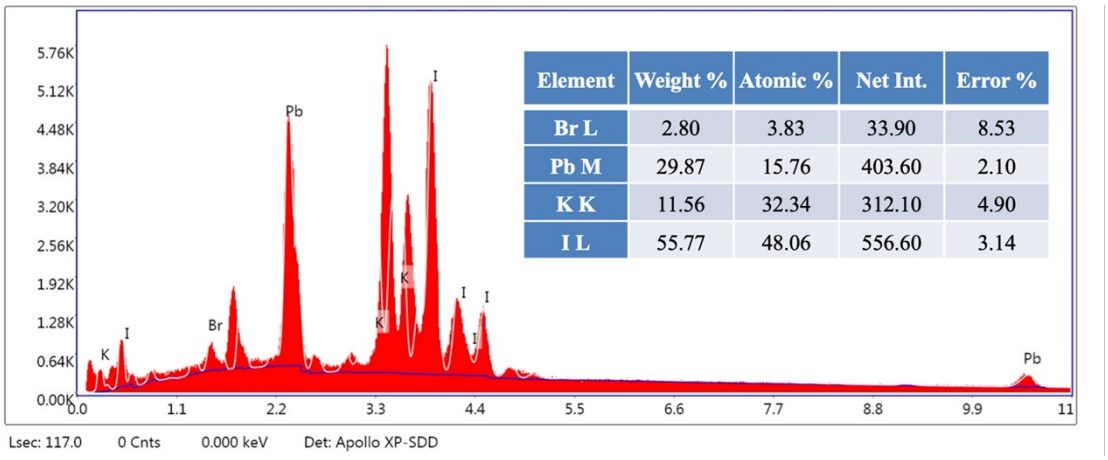

Element	Weight %	Atomic %	Net Int.	Error %
Br L	2.80	3.83	33.90	8.53
Pb M	29.87	15.76	403.60	2.10
K K	11.56	32.34	312.10	4.90
I L	55.77	48.06	556.60	3.14

Fig. S9 EDX elemental spectra of the $(KPbI_3)_{0.05}(FAPbI_3)_{0.9}(MAPbBr_3)_{0.05}$ film (BM). Insert: atomic ratios of elements K, Pb, I and Br.

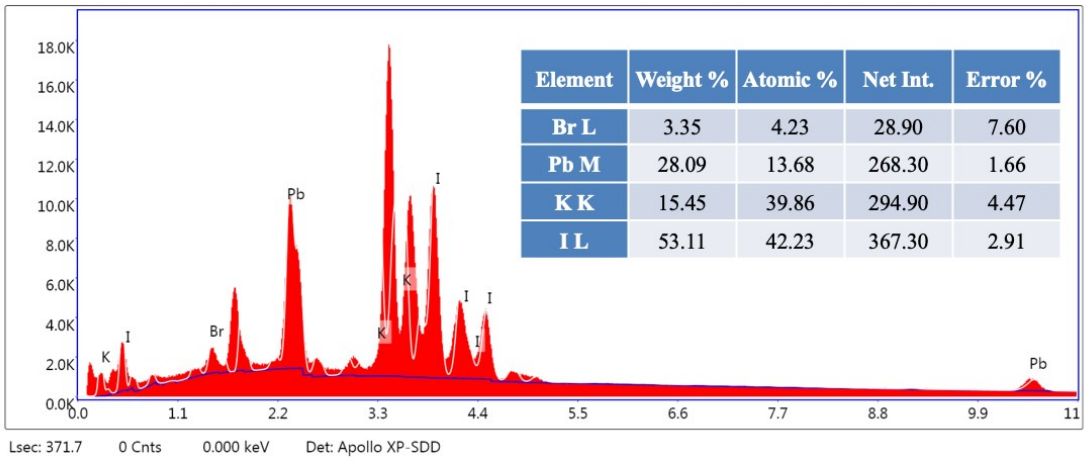

Element	Weight %	Atomic %	Net Int.	Error %
Br L	3.35	4.23	28.90	7.60
Pb M	28.09	13.68	268.30	1.66
K K	15.45	39.86	294.90	4.47
I L	53.11	42.23	367.30	2.91

Fig. S10 EDX elemental spectra of the $(KPbI_3)_{0.05}(FAPbI_3)_{0.9}(MAPbBr_3)_{0.05}$ film (SS). Insert: atomic ratios of elements K, Pb, I and Br.

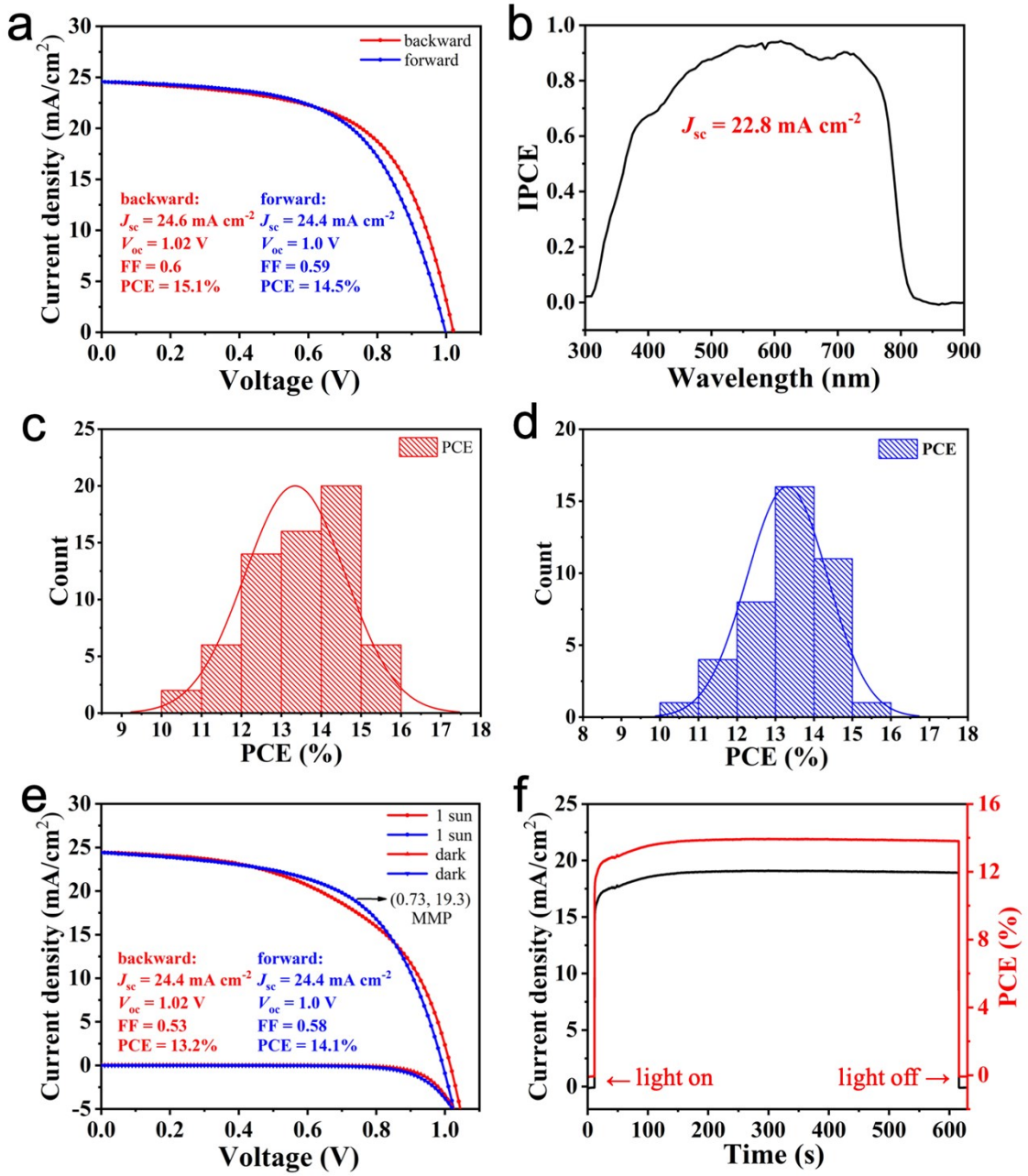

Fig. S11 (a) *J–V* curves of the best performing soalr cell under forward and backward scans by using KI, FAI, PbI_2, MABr and $PbBr_2$ in the corresponding ratio of $(KPbI_3)_{0.05}(FAPbI_3)_{0.9}(MAPbBr_3)_{0.05}$ prepared by SS; (b) IPCE test result and integrated J_{sc} value; cell efficiency distributions; (c) backward scan; (d) forward scan; (e) *J–V* curves of the cell for steady-state output test; (f) steady-state current density and PCE continuous output of the tested cell at MMP for 600 s.

Fig. S9a shows representative *J–V* curves of PSCs made from the SS method, with a PCE of 14.5% (forward scan, V_{oc}, J_{sc} and FF being 1.0V, 24.4 mA cm^{-2} and 0.59, respectively) and 15.1% (backward scan, V_{oc}, J_{sc} and FF being 1.02V, 24.6 mA cm^{-2} and 0.6, respectively). The IPCE spectrum demonstrates a high photon-to-current conversion efficiency from 400 nm to

800 nm. The integrated current density (22.8 mA/cm^2) obtained from the IPCE spectrum (AM 1.5 G) is well matched to the value (24.4 mA/cm^2) measured from the *J–V* curves (Fig. S9b). Under the optimal conditions, the power conversion efficiency distributions of the obtained devices are shown in Fig. S9c (backward scan) and Fig. S9d (forward scan). The obtained devices have relatively narrow efficiency distributions, which proves that the method has good repeatability. The PCE distribution is 10%−16% for both scans. The average PCEs are 13.0% (backward scan) and 13.3% (forward scan). The stabilised maximum power output measurements presented in Fig. S9e and Fig. S9f show good agreement between the measured PCE and the power output. When applying a constant voltage of 0.73 V corresponding to the MMP, the output current density is stable at 18.9 mA cm^{-2} under the continuous output test for 600 s, and the corresponding power conversion efficiency is 13.8%, thus showing good continuous output stability.

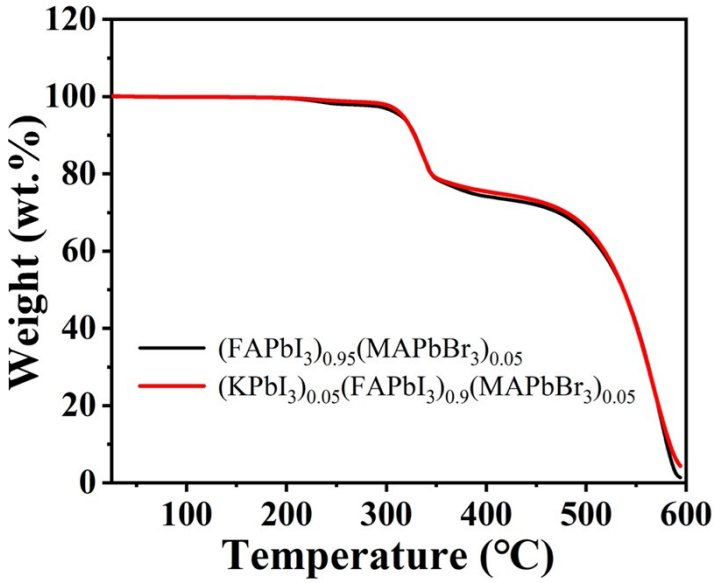

Fig. S12 Thermal stability of the perovskite powders prepared by MCS. TGA curves of (α-$FAPbI_3)_{0.95}(MAPbBr_3)_{0.05}$ and $(KPbI_3)_{0.05}(FAPbI_3)_{0.9}(MAPbBr_3)_{0.05}$.